Accepted to Phys. Fluids 10.1063/5.0173359

A universal scaling law for Lagrangian snowflake accelerations in atmospheric turbulence

Dhiraj K. Singh,[1] Eric R. Pardyjak,[1] and Timothy J. Garrett[2]
[1)]*Department of Mechanical Engineering, University of Utah, Salt Lake City, UT, USA*
[2)]*Department of Atmospheric Sciences, University of Utah, Salt Lake City, UT, USA*

(*Electronic mail: tim.garrett@utah.edu)

(Dated: 29 October 2023)

We use a novel experimental setup to obtain the vertical velocity and acceleration statistics of snowflakes settling in atmospheric surface-layer turbulence, for Taylor microscale Reynolds numbers (Re_λ) between 400 and 67,000, Stokes number (St) between 0.12 and 3.50 and a broad range of snowflake habits. Despite the complexity of snowflake structures and the non-uniform nature of the turbulence, we find that mean snowflake acceleration distributions can be uniquely determined from the value of St. Ensemble-averaged snowflake root-mean-square (rms) accelerations scale nearly linearly with St. Normalized by the rms value, the acceleration distribution is nearly exponential, with a scaling factor for the (exponent) of -3/2 that is independent of Re_λ and St. Kurtosis scales with Re_λ, albeit weakly compared to fluid tracers in turbulence. Gravitational drift with sweeping is observed for $St < 1$. Surprisingly, the same exponential distribution describes a pseudo-acceleration calculated from fluctuations of snowflake terminal fall speed in still air. This equivalence suggests an underlying connection between how turbulence determines the trajectories of particles and the microphysics determining the evolution of their shapes and sizes.

I. INTRODUCTION

The terminal velocity V_t of a falling particle is determined by a balance between the gravitational force and fluid drag. No comprehensive theory has yet been developed to describe how particles settle within flows that are oscillating or turbulent[1], where particles do not necessarily act as pure fluid tracers but instead can cross Lagrangian fluid trajectories[2–4]. Numerical simulations and laboratory experiments show that both negative and positive perturbations from the terminal velocity are possible, termed 'loitering' and 'sweeping', respectively. Particles of fixed size falling in isotropic turbulence can have an average ensemble settling velocity V_v many times slower or faster than V_t[5].

The question of how turbulent motions affect inertial particles has been considered in fields as diverse as planet formation[6], pulverized coal ash deposition[7], spore transport[8], wildfire brand transport[9], and natural particle deposition in the oceans[10,11]. Snowflakes in a turbulent atmosphere represent a particularly complex example. Predictions of weather and climate models, hurricane trajectories, cloud lifetimes, and atmospheric convective dynamics, all have been found to have strong sensitivity to representations of how fast snowflakes fall, but only by considering spread in V_t rather than V_v[12–18].

This seeming omission owes in part to the challenge of determining how precipitation particles with high structural variability[19] respond to air currents, as well as the non-uniform nature of atmospheric flows[20]. In still air, the speed at which frozen precipitation particles settle has been shown to be modified by their turbulent wakes which induces such phenomena as flutter, spiraling and drifting[21–25]. Adding the complication that the atmosphere is turbulent – which is always the case to some degree – there are few observational studies available to provide guidance. Those that have investigated the problem did so by imaging snowflake passage through a light sheet. They inferred that sweeping motions dominate particle dynamics rather than loitering[26,27]. Notably, however, assessment of the snowflake inertial properties was limited by an absence of concurrent measurements of snowflake density and mass.

Turbulence intensity and the interactions between turbulence and inertial particles are commonly defined using two dimensionless parameters: the turbulent Taylor microscale Reynolds number $R_\lambda = u'\lambda/\nu$, where u' is the root-mean-squared (rms) along-wind velocity and λ is the Taylor length scale of turbulence, and the Stokes number $St = \tau_p/\tau_\eta$, where τ_p and τ_η are the particle-response time scale and Kolmogorov time scale, respectively. Note that Taylor microscales computed using three-dimensional sonic anemometers should be viewed with caution, as the measurement scale of the anemometer can be of the same order as the microscale. However, the integral length scale L_u of the largest eddies in the flow can also be estimated based on the temporal autocorrelation function of the streamwise turbulent velocity fluctuations, which offers a more reliable length-scale parameter for experimentally characterizing turbulence in the atmospheric surface layer. The particle settling timescale is given by $\tau_p = V_t/g$, where V_t accounts for non-linear drag associated with particle Reynolds numbers greater than unity and g is the acceleration due to gravity. The Kolmogorov timescale is determined from $\tau_\eta = (\nu/\varepsilon)^{1/2}$ where ν is the kinematic viscosity and ε the dissipation rate of turbulence kinetic energy. Two additional nondimensional parameters include a modified version of the Stokes number $Sv = V_t/u'$ and the density ratio $\beta = 3\rho_f/(\rho_f + 2\rho_s)$, where ρ_f and ρ_s are the surrounding air and snowflake densities[28], respectively. Computation of ρ_s is non-trivial [29] and the method used herein is described in detail in[30].

In this work, we present an experimental study of the Lagrangian dynamics of the vertical acceleration, extreme acceleration, kurtosis, and acceleration variance statistics for a wide range of measured snowflake sizes and densities for at-

Accepted to Phys. Fluids 10.1063/5.0173359

mospheric turbulence with Reynolds numbers spanning 400 to 67,000 and ensemble mean Stokes numbers between 0.12 and 3.50. The structure of this paper is as follows: in Section II, we describe the experimental facility and data analysis. The classification of snowflakes is described in Section III. The results are presented in Section IV, followed by a conclusion in Section IV.

II. EXPERIMENTS AND DATA ANALYSIS

For the study here, we introduce to studies of snowflake settling a new device developed for the direct measurement of hydrometeor mass, size, and density – the Differential Emissivity Imaging Disdrometer (DEID)[31] (See Appendix A). During a series of field experiments conducted at a high-elevation mountain location in Utah between October 2020 and April 2021[32], the DEID was deployed alongside measurements of air temperature, relative humidity and turbulence, and placed directly beneath a particle tracking system consisting of a laser light sheet and a single-lens reflex (SLR) camera. All measurements were made at a nominal height of 2 m above the top of the snowpack level (see Fig. 1a), and the schematic of the experimental setup is illustrated in Fig. 1b. The particle tracking system consisted of a laser sheet with a sampling volume of 10 cm $\times$ 18 cm $\times$ 7 cm oriented normal to the viewing angle of a Nikon D850 SLR camera. Snowflake tracking was performed using a Particle Tracking Velocimetry (PTV) technique[33,34] to measure particle vertical velocities V_v in the laser light sheet for concentrations between 1500 m^{-3} and 2800 m^{-3} (Fig. A1a) and Particle Streak Velocimetry (PSV)[35] for concentrations between 710 m^{-3} and 1460 m^{-3} as illustrated in Fig. A1a. The SLR camera recorded 1920 pixel $\times$ 1080 pixel images with a spatial resolution of $\approx$ 160 μm pixel^{-1} at 120 fps within a vertical laser sheet created using three 10 W, 520 nm diode lasers and a collimator lens. A laser-beam spread angle of $\approx 6.8^\circ$ allowed for a light sheet with near constant thickness of $\approx$7 cm throughout the region of interest. A single focal length Nikon AF-S VR Micro - Nikkor 105 mm f/2.8G IF-ED lens permitted a depth of field greater than the thickness of the laser sheet.

Particle vertical velocities V_v and accelerations a_v were measured within the laser sheet, which could be subsequently compared to estimates of particle terminal velocities in still air V_t derived from DEID microphysical measurements and well-known aerodynamic formulations[36,37] (see Appendix B)

III. CLASSIFICATION OF SNOWFLAKE HABIT

Snowflake images from the particle tracking system and the DEID are used together to classify snow-crystal type following the method outline by[38] following the international classification for seasonal snow on the ground[39]. Mathematically, SDI is defined as the ratio of a snowflake's area directly measured by the DEID, A_s to the melted area of a spherical water

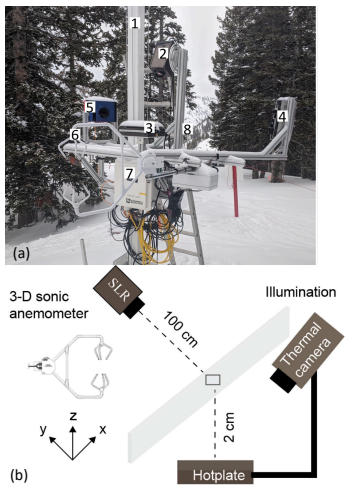

FIG. 1. (a) Experimental setup for measurement of the microphysical properties of snowflakes and their motions. (1) 20m tower (2) Infrared camera (3) DEID Hotplate (4) Three 10-W lasers and optical lens (5) D850 Nikon SLR camera (6) 3D sonic anemometer (7) Data logger/computer and (8) Relative humidity and temperature sensor. (b) Schematic of setup used for measurement of turbulence and snowflake velocity.

droplet, A_w with the same mass (Eq. 1),

$$\mathrm{SDI} = \frac{A_s}{A_w}. \tag{1}$$

The melted area of a spherical droplet is estimated using the snowflake's mass and can be expressed as

$$A_w = (\frac{9\pi}{16})^{1/3} \left(\frac{m}{\rho_w}\right)^{2/3}. \tag{2}$$

Here, m is the mass of the snowflake, and ρ_w the density of liquid water, which is taken to be 1000 kg m^{-3}.

An SDI = 1 corresponds to a spherical rain drop, and high values of SDI indicate a more complex snowflake structure and hence lower snowflake density. The range of SDI for six snowflake types is illustrated in Fig. 2 and the range of SDI for the five cases shown in Table II. The probability distribution function of SDI for five cases is plotted in Fig. 3.

IV. RESULTS

Ten case studies are considered here, each lasting between approximately 3 and 15 minutes, encompassing a total sample of 533,000 snowflake particles. As summarized in the Table I, our measurements cover a particularly broad range of turbulence and microphysical conditions compared to prior

Accepted to Phys. Fluids 10.1063/5.0173359

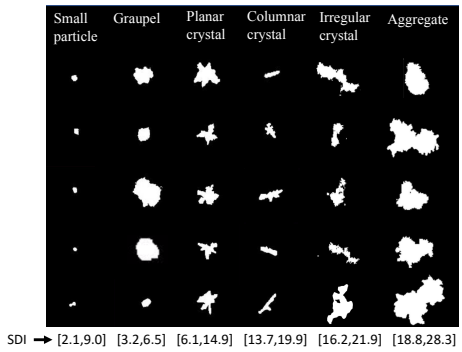

FIG. 2. Binary snowflake images obtained from a particle tracking system, along with the range of associated SDI for each category. Each type consists of five samples.

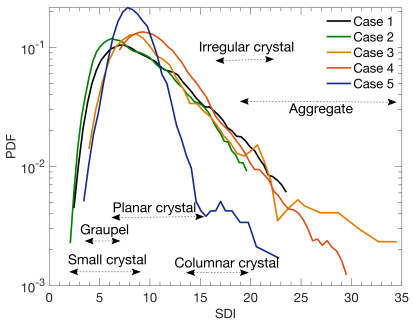

FIG. 3. Probability distribution of SDI for five cases summarized in Table II along with the associated range of values of SDI shown in Fig. 2.

studies of interactions between particles and turbulence: most notably three orders of magnitude in R_λ and three orders of magnitude in St, with values of R_λ between 400 and 67,000 and values of St between 0.01 to 12.00, and also the first direct measurements of snowflake density varying between 9 and 285 kg m^{-3}[30]. Snowflake effective diameter $D_{\rm eff}$ ranged from 0.5 mm to 11.9 mm (see Fig. A2a) and aspect ratios between 1.0 and 9.3. Snowflake settling velocity V_v and terminal velocity V_t ranged from -2.13 to 4.21 ms^{-1} and from 0.06 to 3.24 ms^{-1} respectively and PDFs of V_v and V_t for a particular case is shown in Fig. A2b. Five representative case studies are considered here, each lasting between approximately 3 and 15 minutes, encompassing a total sample of 335,000 snowflake particles. As summarized in the Table II, the mean values of each parameter include values of R_λ between 400 and 67,000, values of St between 0.12 to 3.51, integral length scales L_u varying from 11 m to 198 m, and mean snowflake densities between 54 and 87 kg m^{-3}. Snowflake mean settling velocities ranged from 0.11 to 0.76 ms^{-1} and their mean terminal velocities from 0.43 to 0.64 ms^{-1}.

Figure 4a shows examples of snowflake dynamics in turbulence. Falling particles may be unperturbed by turbulent eddies when they are dense with low values of β and high values of St, but can display quite chaotic trajectories when β is high and St is low (following trajectories associated with turbulent eddies more faithfully). Settling velocities in Fig. 4b shows not only sweeping as was previously observed[26,27] but also significant loitering. The highly asymmetric nature of the settling-velocity distribution relative to terminal velocities (in still air) suggests that the effect of turbulence on snowflake velocities does not simply average to zero. In other words, it cannot be assumed that the terminal velocity is a satisfactory ensemble approximation of the mean settling velocity.

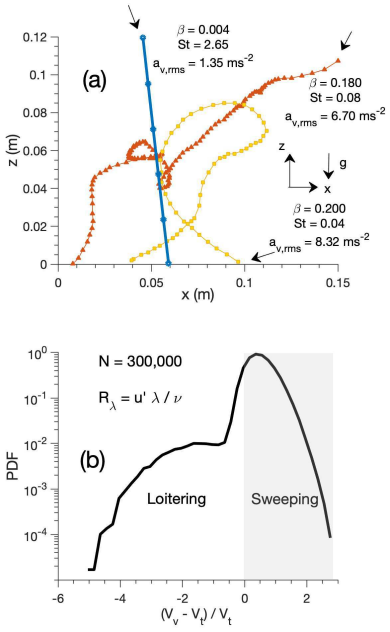

FIG. 4. (a) The trajectories of snowflakes with three distinct values of β, $a_{\rm rms}$, and St but the $\approx$ same area sampled during a three-minute period where $R_\lambda = 690 \pm 49$. The trajectory shown by a black line covers a duration of 0.7 τ_η and the red line a duration of 28 τ_η. Arrows indicate the starting position of each snowflake. (b) The probability distribution function of the relative difference of snowflake settling velocity to the terminal velocity during a three-minute event with approximately N = 300,000 snow particles in turbulence with $R_\lambda = 2500 \pm 200$ and $St_m = 0.64 \pm 0.26$. Note that positive values of V_t andV_v indicate downward snowflake motion.

Here, we are primarily concerned with evaluating the mechanisms that determine departures from the terminal velocity, or snowflake vertical accelerations. Experimentally, these accelerations a_v can be calculated from fluctuations in snowflake velocities observed using particle tracking, calculated here by differentiating a third-order polynomial fit to the times series of snowflake velocities and evaluated over a duration equivalent to the Kolmogorov time scale τ_η[40] (see Appendix B). The Kolmogorov time scale ranges from 0.02 s to 0.24 s depending on turbulence levels. Figure 5 shows measured acceleration distributions normalized with respect to the rms value $a_{v,\mathrm{rms}} = \langle a_v^2 \rangle^{1/2}$ for five case-study periods characterized by R_λ varying from 400 to 67000 and St varying from 0.12 to 3.50. The distribution closely approximates a Laplacian, namely an exponential distribution symmetric about $0\,\mathrm{m\,s^{-2}}$. The exponent slope with respect to $|a_v|/a_{v,\mathrm{rms}}$ is nearly $3/2$ (Fig. 5a), for all R_λ and St, a scaling noted previously in Lagrangian simulations looking at spherical particles with $Re_\lambda \sim \mathcal{O}(100)$[41].

More notably, we find that an equivalent Laplacian distribution represents another pseudo-acceleration ($\hat{a}_t$) calculated from a second-order polynomial fit to Eulerian fluctuations in the ensemble-mean snowflake terminal velocities $\langle V_t \rangle$. That is, $\hat{a}_t$ is an acceleration calculated from a time series of ensemble-averaged terminal velocities of snowflakes that have fallen onto the hotplate (Appendix B).

This result is particularly surprising given that *a priori* the terminal velocity would be seen as being independent of local turbulence. It is determined uniquely by spatial and temporal variability in snowflake mass, size, and density, and is therefore primarily a function of microphysical growth processes in clouds aloft. Even though the Lagrangian accelerations collapse onto a single distribution curve, the cumulative distribution in Fig. 5b indicates that $\approx 10\%$ more of the normalized accelerations are greater than unity for the highest R_λ compared to the lowest R_λ. Hence, the likelihood of extreme accelerations is significantly greater for the largest Reynolds numbers.

The observed universality in the mathematical relationships characterizing the temporal Lagrangian velocity variability of individual snowflakes and Eulerian terminal velocity variability of snowflake ensembles is consistent across the full range of turbulence and snowflake events measured (Fig. 5a). Generally, the slope of a log-log plot of the Laplacian distribution with respect to the positive value $|a_v|/a_{v,\mathrm{rms}}$ is -1.5 ± 0.05, where the normalization of the Laplacian distribution scales with turbulence intensity as $a_{v,\mathrm{rms}} \propto R_\lambda^{0.64}$ and $a_{v,\mathrm{rms}} \propto St^{0.98}$ (see Fig. 6). The nearly linear increase of snowflake $a_{v,rms}$ with the mean of the St distribution in Fig. 6a appears to be at odds with prior studies (e.g., Bec et al.[41]) that show $a_{v,rms}$ decreasing with increasing St for a fixed value of R_λ. Note, however, that for calculations of St in Fig. 6, the mean τ_p varies far less than τ_η so the results primarily reflect variability in turbulence through R_λ. More detailed particle-by-particle experiments will be required to examine how $a_{v,rms}$ varies with St for the case that R_λ is fixed but individual snowflake terminal velocities – and τ_p – vary more extensively than seen in the mean values presented here. The maximum of the normal-

TABLE I. Minimum and maximum values of snowflake and turbulence parameters measured using the DEID, a sonic anemometer and particle tracing velocimetry. U - mean wind speed, λ - Taylor microscale, ε - turbulence kinetic energy dissipation rate, R_λ - Reynolds number based on the Taylor microscale, D_{eff} - snowflake diameter, ρ_s - snowflake density, AR - aspect ratio, V_t - snowflake terminal velocity, V_v - snowflake measured vertical fall velocity, St - Stokes number, and Sv - modified version of the Stokes number.

Parameter	Minimum	Maximum
U (m s^{-1})	0.09	6.52
λ (mm)	23	632
ε (cm^2/s^3)	0.15	316.
R_λ	400	67000
D_{eff} (mm)	0.5	11.9
ρ_s (kg m^{-3})	9	285
AR	1.0	9.3
V_t (m s^{-1})	0.06	3.24
V_v(m s^{-1})	- 2.13	4.21
St	0.01	12
Sv	0.03	18

TABLE II. Snowflake and turbulence characteristics measured using the DEID, a sonic anemometer, and particle tracing velocimetry for five case studies: Case 1, February 16, 2021; Case 2, December 12, 2020; Case 3, January 4, 2021; Case 4, December 18, 2020; Case 5, March 16, 2021. U - mean wind speed, σ_u - standard deviation of streamwise velocity fluctuations, σ_w - standard deviation of vertical velocity fluctuations, L_u - integral length scale computed from streamwise velocity fluctuations, λ - Taylor microscale, ε - turbulence kinetic energy dissipation rate, R_λ - Reynolds number based on the Taylor microscale, D_{eff} - snowflake diameter, ρ_s - snowflake density, AR - aspect ratio, V_t - snowflake terminal velocity, V_v - snowflake measured vertical fall velocity, St - Stokes number, and Sv - modified version of the Stokes number, Δt - duration of each case, T - ambient temperature, RH - relative humidity, N - total number of snowflakes in each case.

Parameters	case1	case2	case3	case4	case5
U (m s^{-1})	2.26	1.73	1.18	0.72	0.29
σ_u (m s^{-1})	1.62	0.96	0.72	0.42	0.11
σ_w (m s^{-1})	0.42	0.47	0.21	0.26	0.06
L (m)	198	92	161	41	11
λ (mm)	632	411	378	201	65
ε (cm^2/s^3)	356	467	130	48	7
R_λ	67000	24000	22000	5800	400
D_{eff} (mm)	2.1	1.5	1.2	1.4	1.5
ρ_s (kg m^{-3})	87	68	79	64	54
AR	1.28	1.30	1.17	1.21	1.34
V_t (m s^{-1})	0.57	0.47	0.43	0.48	0.64
V_v(m s^{-1})	0.11	0.21	0.18	0.53	0.76
St	3.51	1.68	1.54	0.64	0.12
Sv	0.21	0.28	0.38	1.02	2.85
SDI	[2.1,23.5]	[2.0,19.6]	[3.9,34.9]	[6.9,29.5]	[3.4,22.5]
Δt (min)	3	15	7	6	7
T (°C)	-10	-11	-5	-7	-6
RH (min)	96	97	95	95	96
N (min)	126,000	129,689	34,000	21,000	25,000

Accepted to Phys. Fluids 10.1063/5.0173359

ized distribution of acceleration is only weakly dependent on turbulence intensity, increasing by $\approx 2\%$ over three orders of magnitude in R_λ.

An interesting exception to the Laplacian vertical acceleration distribution is how fat tails that encompass $\approx 1\%$ of the total ensemble appear to be related to particularly porous hydrometeors that occupy the bottom 1% of the density distribution, having an average density of 12.9 kg m^{-3} or $\beta = 0.102$.

The maximum Lagrangian snowflake acceleration (extreme a_v) measured during this study was an astonishing 142 m s^{-2}, 15 times the $a_{v,\mathrm{rms}}$ value, and ≈ 14 times the acceleration of gravity. While the 1.85 mm particle diameter of this "lucky" snowflake was unremarkable, the associated snowflake density had a low value of 12.7 kg m^{-3}. For the measured snowflake ensemble, extreme values of a_v scaled as $0.27R_\lambda^{0.56}$ (Fig. 6b). The observations indicate that such extreme ac-

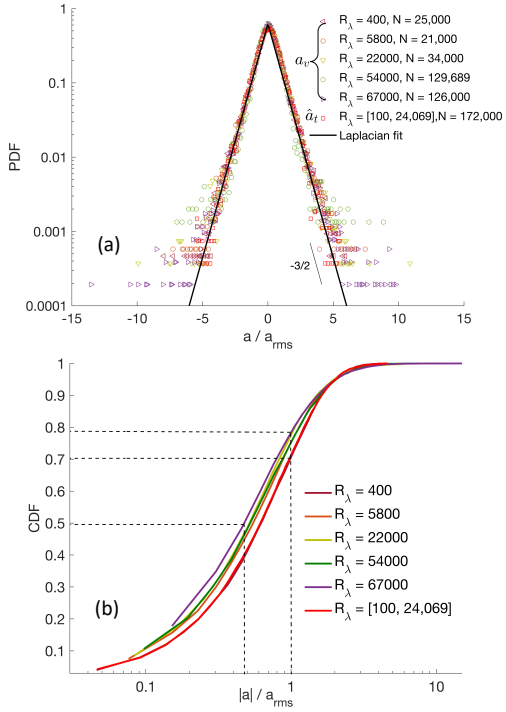

FIG. 5. (a) Normalized vertical acceleration distributions. Probability distribution of vertical accelerations a_v binned by 0.1 m s^{-2} and normalized by $a_{v,\mathrm{rms}}$ for a range of Reynolds numbers R_λ and Stokes numbers St calculated for periods ranging in duration from approximately 3 minutes to 15 minutes. Eulerian pseudo-accelerations ($\hat{a}_t$) calculated from the ensemble mean terminal velocity inferred from DEID measurements of particle size, mass, and density. The solid line represents a Laplacian fit for the case where R_λ = 67000 and St = 3.50. The solid-line fit characterizes the normalized vertical acceleration with a Laplacian function $P(\hat{a}) = C_1 exp(-C_2|\hat{a}|)$ where $\hat{a} = a/a_{\mathrm{rms}}$, C_1 is the maximum of the probability distribution function, and $C_2 = 1.5 \pm 0.05$, or approximately 3/2. We define the Laplacian distribution's scaling (exponent) as $-C_2$, the slope of the positive domain of the normalized acceleration distribution curve plotted on a log-log scale. Hence the scaling exponent is -3/2. The results point to universality of an acceleration frequency distribution scaling as -3/2 $\pm$ 0.05 a/a_{rms}. (b) Normalized cumulative distribution function of vertical accelerations.

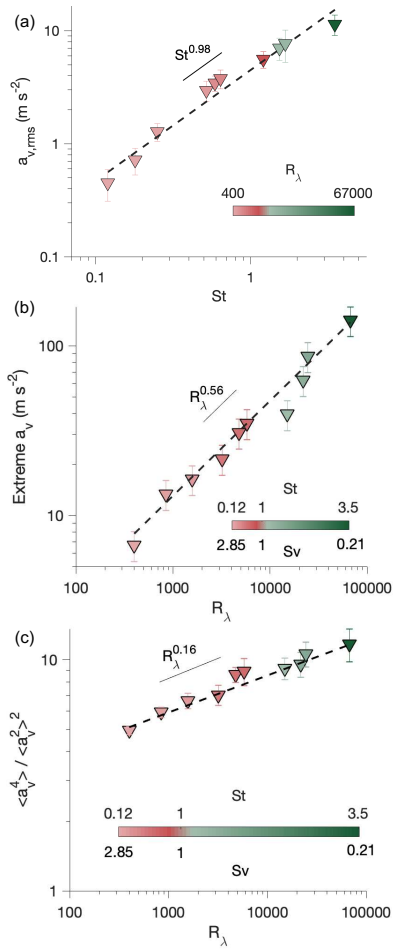

FIG. 6. (a) Shows the root-mean-squared vertical acceleration $a_{v,\mathrm{rms}}$ as a function of St. (b) Extreme values of the Lagrangian acceleration (a_v) vs. Reynolds number and (c) the flatness K vs. Reynolds number color-coded for acceleration and Stokes number (St, Sv). Bars represent systematic and random uncertainties in the extreme values of $a_{v,\mathrm{rms}}$, a_v and in K due to measurement error in V_v.

celerations appear when typically low-density snowflakes become trapped in a vortex and then are later kicked out (Fig. 4a).

Departures from Gaussian and Laplacian distributions have previously been associated with intermittent particle accelerations. Unusually rare but large particle-acceleration events arise due to turbulence[42]. Their frequency can be represented mathematically by the acceleration distribution flatness or kurtosis $K = < a_v^4 > / < a_v^2 >^2$, or the fourth moment of the normalized acceleration distribution. $K = 3$ for a Gaussian distribution and $K = 6$ for a Laplacian distribution. For snowflakes, we observed that flatness scales monotonically with turbulence, but only weakly so. Specifically, flatness ranges from approximately 5 to 12 following the functional forms $K = 1.95R_\lambda^{0.16}$ and $K = 9.02St^{0.25}$ (Fig. 6c).

As a reference point, fluid tracers with large values of β have values of K that are an order of magnitude larger[43] because the response to turbulence is stronger. In idealized laboratory experiments, $K = 4R_\lambda^{0.41}$[40,44] for fluid tracers and $K = 6R_\lambda^{0.29}$ for micro-bubbles[45]. Numerical simulations suggest that heavy spherical particles with large values of St respond more slowly than near-fluid tracers to variations in the fluid flow. They cannot attain extremely high accelerations due to inertial filtering[41]. Values of K still scale weakly with turbulence intensity, but maintain a value near the Laplacian value of 6, nearly independent of particle size and density[46,47], at least for weaker turbulence with $R_\lambda \lesssim 100$. Instead they suggest that the acceleration distributions of snowflakes, as dense particles responding to non-idealized turbulent flows, are consistent with prior numerical studies pointing to low flatness. They further extend the applicability of assuming a near-Laplacian distribution to particles that are irregularly shaped and to values of R_λ as high as 67,000.

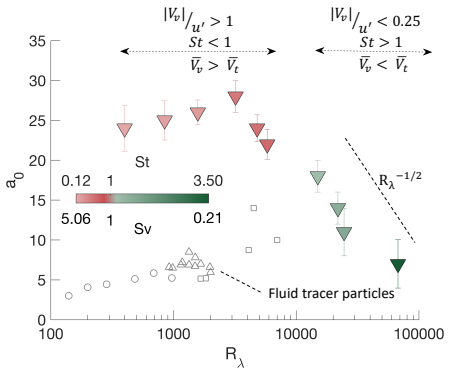

FIG. 7. The Heisenberg-Yaglom constant a_0 for snowflakes as a function of R_λ, St_m and Sv. For comparison, fluid tracer particles in homogeneous turbulence obtained by[40,44] (circles) and[48] (squares) and measured by hot-wire anemometer in air[49] (triangle). The error bars represent the systematic and random errors in measurements of snowflake acceleration variance.

With respect to values of $a_{v,\mathrm{rms}}$, we observe snowflakes have a nearly linear scaling with St that deviates considerably from prior results describing $a_{v,\mathrm{rms}}$ for fluid tracers. The Heisenberg-Yaglom formula is widely used to express Lagrangian root-mean-square particle accelerations in terms of the acceleration at the dissipative spatial scale, that is $a_\eta^2 = \nu^{-1/2}\varepsilon^{3/2}$[50]. The general expectation is that $a_{v,rms}^2 = a_0 a_\eta^2$. The Kolmogorov constant a_0 represents the non-dimensional variance of the particle acceleration, and is equal to unity for Gaussian fluctuations[51]. Deviations from unity arise due to intermittency in turbulence and particle properties[40,52]. Here, values of a_0 are calculated over a fit interval time (τ_f)[40] (see Fig. A3b). Fig. 7 indicates that for the case that St < 1 values of a_0 are many times higher than those described previously for fluid tracers in isotropic homogeneous turbulence[40,44,48,49,53]. We hypothesize this discrepancy owes to gravitational drift (the ratio of snowflake fall speed to the characteristic speed of air velocity fluctuations) and sweeping[54,55]. For St < 1, we see high observed ratios of snowflake settling speed to the characteristic speed of the air-velocity fluctuations $|V_v|/u' > 1$, and also for average settling speeds relative to terminal fall speeds $\overline{V}_v/\overline{V}_t > 1$.

Fig. 7 shows also, for the case of heavier particles with $St_m > 1$ (or $Sv < 1$), that a_0 decreases with R_λ, scaling as $a_0 \propto R_\lambda^{-1/2}$. This result lies in sharp contrast with prior experimental and numerical work for fluid particles in homogeneous turbulence showing that a_0 increases monotonically with R_λ, albeit only when considering turbulence levels with $R_\lambda < \mathcal{O}(10^4)$. For snowflakes in this Stokes-number regime, gravitational drift is weaker, and is associated with measured $|V_v|/u' < 0.25$ and loitering with $\overline{V}_v/\overline{V}_t < 1$).

At $St \sim \mathcal{O}(1)$ and $R_\lambda > \mathcal{O}(10^4)$, heavier particles start detaching from the fluid streamlines. As a result, a_0 decreases with further increases in R_λ. Note that the change in St is only due to a change in turbulence levels because particle characteristic time scales are approximately the same in all cases. The acceleration variance constant is known to deviate from unity due to intermittency[56]. Our results show that intermittency in Lagrangian acceleration has a different trend for values of St lower and higher than unity and for $R_\lambda \approx \mathcal{O}(10^4)$. An explanation for this phenomenon remains an open problem.

V. CONCLUSION

Summarizing, highly-asymmetric snowflakes settling in complex irregular turbulent flows behave very differently from fluid tracers but nonetheless obey remarkably simple mathematical relations. They exhibit sweeping for $St < 1$ with high constant values of the Kolmogorov constant a_0, and loitering for $St > 1$ with a_0 scaling as $R_\lambda^{-1/2}$. Spanning over three orders of magnitude of variation in the turbulent Reynolds number, Lagrangian vertical velocity fluctuations have a universal frequency distribution of $\exp[-3a_v/(2a_{v,rms})]$, independent of R_λ, where $a_{v,rms}$ scales linearly with St. Stated another way, snowflake acceleration distributions could in prin-

ciple be uniquely inferred given only a measure of the Stokes number. Moreover, the ensemble-mean terminal velocity – a quantity that is a function only of snowflake mass and shape – has the same fluctuation statistics. The similarity in scaling relationships would not have been observed had the particle properties been prescribed, as for example they would be in laboratory or numerical simulations. In field measurements, the observation was only made possible through the use of a novel disdrometer designed for measurement of snowflake microphysical properties.

Snow scientist U. Nakaya famously termed snow crystals photographed at the ground "letters from the sky"[57] because their delicate structures carry information about temperature and humidity fluctuations higher up in the clouds where crystal basal and prism facets competed for water vapor deposition. The observed correspondence between acceleration and pseudo-acceleration distributions may simply point to a similar message. In general, faster updrafts in clouds lead to larger snowflakes that fall with higher terminal velocities because more time is available to sustain snowflake growth through aggregation and supercooled cloud droplet riming. In this vein, given the shape of acceleration distributions is invariant with turbulence levels, it seems possible that snowflake terminal velocity variability measured at the ground simply reflects that within turbulent clouds higher up[58]. It remains to be shown what precise mechanism leads to such a close correspondence between snowflake Lagrangian accelerations and terminal velocity pseudo-accelerations, or for that matter why the precise value of the scaling in the exponent is $-3/2$.

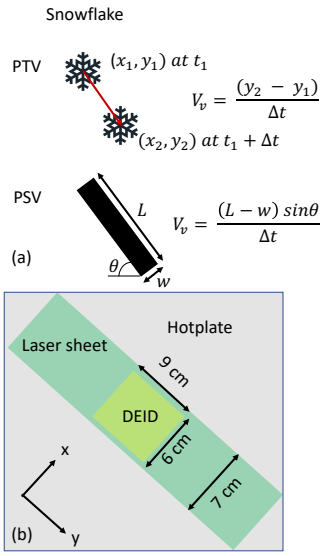

FIG. A1. Methodology for calculation of the snowflake velocities (a) Particle Tracking Velocimetery (PTV) procedure comparing snowflake position between two frames and a Particle Streak Velocimetery (PSV) procedure for tracking individual snowflakes within one frame. x_1, y_1 is the centroid of a snowflake at time t_1, and x_2, y_2 is the centroid at time t_1+Δt, where Δt is the time interval between two frames. L is the total snowflake displacement in time Δt, and w is the snowflake dimension normal to its direction of motion, which is unaffected by the camera exposure time. The fall angle is θ. In this paper, only PTV is used for acceleration calculation. (b) Top-view of the laser system and DEID showing co-location of these two instruments for matching snowflake velocity measurements to their microphysical properties.

ACKNOWLEDGMENTS

We appreciate constructive comments from reviewers Michele Guala and Raymond Shaw. We thank Allan Reaburn and his colleagues at Particle Flux Analytics, Inc. for their contributions to the development of the DEID, Dave Richards and the Alta Ski Patrol for field support, and Spencer Donovan for contributions to the experimental setup. This material is based upon work supported by the National Science Foundation under Grant Nos. PDM-1841870 and PDM-2210179.

AUTHOR DECLARATIONS

Conflict of interest

The DEID technology is protected through patent US20210172855A1 co-authored with D.K.S., E.R.P., and T.J.G. and is commercially available through Particle Flux Analytics, Inc. T.J.G. is a co-owner of Particle Flux Analytics, Inc. which has a license from the University of Utah to commercialize the DEID.

Author Contributions

T.J.G. and E.R.P. conceived the study; D.K.S., E.R.P. and T.J.G. designed the experiments and D.K.S performed the experiments in consultation with E.R.P and T.J.G.; All authors analyzed the data and contributed to writing and editing the paper.

DATA AVAILABILITY STATEMENT

The data that support the findings of this study are available from the corresponding author upon reasonable request.

Appendix A: Microphysical measurement of snowflakes

Accepted to Phys. Fluids 10.1063/5.0173359

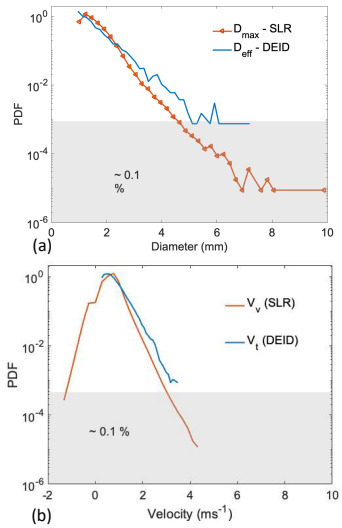

FIG. A2. (a) Nearly equivalent size distributions of snowflakes with respect to D_{max} measured by the D850 Nikon camera in the x-z plane and of D_{eff} measured by the DEID in the x-y plane. (b) Distributions of actual fall velocity (V_v) measured in the x-z plane, where negative upward velocity represents loitering and of the terminal velocity (V_t) is estimated from the x-y plane using DEID measurements of hydrometeor microphysical properties. The shaded region encompasses the bottom $\approx 0.1\%$ of the frequency distribution.

Details of the microphysical measurements are given in Singh et al.[31]. Briefly, the DEID disdrometer consists of an infrared camera pointed at a low-emissivity heated metal plate[31,59]. To compute a snowflake's area on the hotplate, the DEID makes use of the contrasting thermal emissivities of water (> 0.95) and aluminum (< 0.1). While the brightness temperature of the water and aluminum rapidly equilibrate, the two materials have different brightness temperatures. As a result, hydrometeors appear as bright regions on a dark background in the thermal-camera imagery and geometric quantities such as snowflake area as easy to calculate. For this study, the DEID's spatial resolution is approximately 200 μm pixel^{-1}. Measurement of the mass of an individual hydrometeor uses gray-scale imagery of the particle area, the temperature difference between the hydrometeor on the plate and the hotplate, and the evaporation time. Individual snowflake mass is determined assuming that the heat gained by a hydrometeor is equivalent to the heat lost by the hotplate during the complete evaporation. Our wind-tunnel studies found that mass measurements are nearly independent of environmental conditions, including wind, relative humidity, and ambient temperature.

Appendix B: Terminal velocity estimation

The DEID provides direct measurements of the mass of individual hydrometeors (m), their circumscribed area (A), and their area on the plate (A_e). See[31,38] for details. A is calculated using the smallest circle or ellipse drawn around the area (A_e). The equivalent circular diameter of a snowflake (D_{eff}) is defined as $A_e = (\pi/4)D_{eff}^2$. From these parameters, individual snowflake-equivalent still-air terminal velocities can be estimated using an aerodynamic formula[36]:

$$V_t = \frac{Re \cdot \eta}{2\rho_a}\left(\frac{\pi}{A_e}\right)^{1/2}, \tag{B1}$$

where ρ_a and η are the density and dynamic viscosity of air, respectively. The Reynolds number is parameterized as

$$Re = 8.5[(1+0.1519X^{1/2})^{1/2} - 1]^2, \tag{B2}$$

where X is determined from atmospheric environment data and snow particle properties as

$$X = \frac{8mg\rho_a}{\pi\eta^2}\left(\frac{A_e}{A}\right)^{1/4}. \tag{B3}$$

A modification to Eq. B2 was suggested by[37], for all natural ice particles, where

$$R_e = 8.5\,[(1+0.48X^{1/2})^{1/2} - 1]^2. \tag{B4}$$

The estimated V_t using Eq. B4 is reduced by $\approx 15\%$ compared to[36].

Appendix C: Acceleration calculation

Snowflake accelerations are estimated using two different techniques: (1) Lagrangian tracking of individual snowflake trajectories in the air (a_v), and (2) as a pseudo-acceleration obtained from a time series of the ensemble-mean snowflake terminal velocities measured using snowflakes that have fallen onto the DEID hotplate ($\hat{a}_t$). Method (1) follows a previously developed approach for determining Lagrangian particle accelerations[40,45]; a snowflake's trajectory $z(t)$ can be low-pass filtered by fitting to a third-order polynomial. The filtered position of the i^{th} snowflake at time t is defined as

$$z_i(t) = a_i + b_i t + c_i t^2 + d_i t^3, \tag{C1}$$

where a_i, b_i, c_i and d_i are polynomial coefficients. The Lagrangian velocity and acceleration are respectively the first and second time derivatives of the snowflake trajectory, given by

$$V_{v,i}(t) = b_i + 2c_i t + 3d_i t^2 \tag{C2}$$

and

$$a_{v,i}(t) = 2c_i + 6d_i t. \tag{C3}$$

Accepted to Phys. Fluids 10.1063/5.0173359

The instantaneous particle acceleration (a_v) is calculated from the second time-derivative of a snowflake's trajectory using a fitted third-order polynomial over a time interval of τ_f, equivalent to the Kolmogorov time scale $\tau_\eta = (\nu/\varepsilon)^{1/2}$ determined as a function of the kinematic viscosity ν and the measured turbulence kinetic energy dissipation rate ε computed using frequency-based energy spectral densities $S(f)$ of the streamwise velocity[60] such that $S(f) = \alpha_K (U/2\pi)^{2/3} \varepsilon^{2/3} f^{-5/3}$, where $\alpha_k = 0.55$, f is the frequency, and U is the mean streamwise velocity. A comparison of the variability associated with using different methods used to compute ε, including the above-listed method, is provided by[22,61]. Adopting this technique, no qualitative differences have been observed in the normalized acceleration distribution for fitting times over the range $0.5\ \tau_\eta < \tau_f < 2\tau_\eta$ and we find results similar to[40].

For method (2), pseudo-accelerations ($\hat{a}_t$) are computed over time intervals of $\tau_f = \tau_\eta$ applied to mean terminal velocity variability, obtained from the time series of the spatial mean of the terminal velocities $\langle V_t \rangle$ of snowflakes measured after they have passed through the laser sheet and are deposited on the hotplate. Variability in V_t is measured at the hotplate sampling rate of 15 Hz, from which a time series of mean terminal velocities is fitted using a second-order polynomial over the time interval $\tau_f = \tau_\eta$, which differentiated to estimate pseudo-accelerations ($\hat{a}_t$). The same fitting procedure is used as to compute a_v. $\langle V_t \rangle(t)$ at time t is estimated as follows

$$\langle V_t \rangle(t) = \frac{1}{N} \sum_{i=1}^{N} V_{t,i}. \tag{C4}$$

$V_{t,i}$ is the terminal velocity of the i^{th} snowflake and N is total number of snowflakes that fell on the hotplate at time t. We refer to this as an Eulerian velocity and acceleration because the snowflakes are not tracked as they fall, as in method (1), rather an ensemble velocity value is obtained for a single area of interest defined by the sampling hotplate where snowflakes land and melt.

Appendix D: Smoothing method for snowflake trajectories

The frequency at which data are measured and the corresponding displacement of particles from one frame to the next (Fig, A3c) affect uncertainties in the acceleration measurement. In particle tracking, two different methods of fitting the snowflake trajectories can be used, a polynomial of third order or Gaussian kernel, are used to smooth snowflake trajectories in atmospheric turbulent flows for the purpose of calculating accelerations. The polynomial of third order approach yields values for the scaling of the Laplacian distribution of the normalized acceleration and $a_{v,\mathrm{rms}}$ that are 2.6% and 7.6% smaller than the Gaussian kernel method, respectively based on a time interval of τ_f. In the paper, we only show results obtained by smoothing the snowflake trajectories with a third-order polynomial. The frame-by-frame acceleration for a sample snowflake trajectory is shown in Fig. A3a.

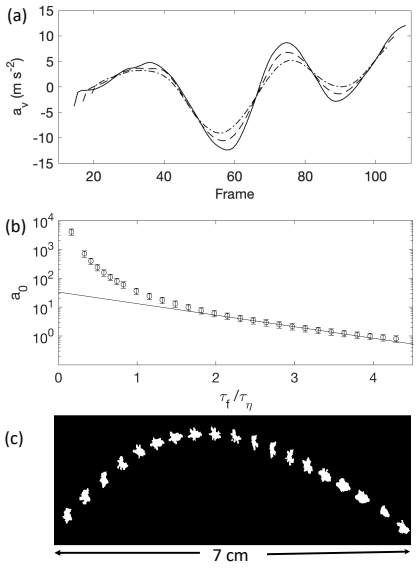

FIG. A3. (a) Frame-by-frame acceleration of a single trajectory of a snowflake estimated with three different third-order polynomial fit times: 30 frames (solid), 35 frames (dashed) and 40 frames (dash-dotted). τ_η is equivalent to 35 frames. (b) Normalized acceleration variance a_0 of the vertical acceleration component as a function of fit interval τ_f normalized by the Kolmogorov time τ_η. The data are taken at $R_\lambda = 400 \pm 38$. The solid line shows the exponential fit extrapolated to $\tau_f/\tau_\eta \to 0$ to provide an estimate of the normalized acceleration variance a_0. We calculate normalized acceleration variance a_0 over a fit interval time τ_η following the approach described by Voth *et al.* [40]. (c) Sample image of a snowflake trajectory.

Appendix E: Systematic and Random error analysis

To obtain uncertainties in the analyses, 554,371 snowflake measurements are considered. Direct measurements made by the DEID include snowflake area, temperature, and evaporation time, for which the respective uncertainties are 1.0%, 0.3%, and 1.0%[31]. The uncertainties in derived quantities (using a standard propagation of uncertainty analysis) such as equivalent diameter (D_{eff}), mass (m), density (ρ_s), and terminal velocity (V_t) are 0.5%, 3.3%, 4.8%, and 3.5%, respectively, neglecting theoretical uncertainties in the formulation used for calculating V_t that are $\approx 15\%$[36,37]. The percentage uncertainty in the settling velocity (V_v) associated with determination of the particle's position owing to camera pixel and time resolution is 6.3%, leading to uncertainties in $a_{v,\mathrm{rms}}$ of 9.4% and average uncertainties in the flatness parameter of 12%, calculated using the *jackknife* algorithm[62].

Accepted to Phys. Fluids 10.1063/5.0173359

[1]J. H. E. Cartwright and O. Piro, "The fluid mechanics of poohsticks," Philosophical Transactions of the Royal Society A: Mathematical, Physical and Engineering Sciences **378**, 20190522 (2020).
[2]M. Yudine, "Physical considerations on heavy-particle diffusion," Adv. Geophy. **6**, 185–191 (1959).
[3]G. Csanady, "Turbulent diffusion of heavy particles in the atmosphere," J. Atmos. Sci. **20**, 201–208 (1963).
[4]M. R. Maxey and J. J. Riley, "Equation of motion for a small rigid sphere in a nonuniform flow," Phys. Fluid. **26**, 883–889 (1983).
[5]G. Good, P. Ireland, G. Bewley, E. Bodenschatz, L. Collins, and Z. Warhaft, "Settling regimes of inertial particles in isotropic turbulence," J. Fluid. Mech. **759** (2014).
[6]L. Pan, P. Padoan, J. Scalo, A. G. Kritsuk, and M. L. Norman, "Turbulent clustering of protoplanetary dust and planetesimal formation," Astro. J. **740**, 6 (2011).
[7]H. Wang and J. N. Harb, "Modeling of ash deposition in large-scale combustion facilities burning pulverized coal," Prog. Energy. Combust. Sci. **23**, 267–282 (1997).
[8]D. E. Aylor, "The role of intermittent wind in the dispersal of fungal pathogens," Annu. Rev. Phytopathol. **28**, 73–92 (1990).
[9]A. Tohidi, *Experimental and numerical modeling of wildfire spread via fire spotting*, Ph.D. thesis, Clemson University (2016).
[10]R. M. Williams, "A model for the dry deposition of particles to natural water surfaces," Atmos. Environ. **16**, 1933–1938 (1982).
[11]J. T. Turner, "Zooplankton fecal pellets, marine snow, phytodetritus and the ocean's biological pump," Prog. Oceanogr. **130**, 205–248 (2015).
[12]S. A. Rutledge and P. V. Hobbs, "The mesoscale and microscale structure and organization of clouds and precipitation in midlatitude cyclones. xii: A diagnostic modeling study of precipitation development in narrow cold-frontal rainbands," J. Atmos. Sci. **41**, 2949–2972 (1984).
[13]S.-Y. Hong, J. Dudhia, and S.-H. Chen, "A revised approach to ice microphysical processes for the bulk parameterization of clouds and precipitation," Mon. Wea. Rev. **132**, 103–120 (2004).
[14]R. G. Fovell and H. Su, "Impact of cloud microphysics on hurricane track forecasts," Geophys. Res. Lett. **34**, L24810 (2007).
[15]D. L. Mitchell, P. Rasch, D. Ivanova, G. McFarquhar, and T. Nousiainen, "Impact of small ice crystal assumptions on ice sedimentation rates in cirrus clouds and gcm simulations," Geophys. Res. Lett. **35**, 9806–+ (2008).
[16]J. A. Finlon, G. M. McFarquhar, S. W. Nesbitt, R. M. Rauber, H. Morrison, W. Wu, and P. Zhang, "A novel approach for characterizing the variability in mass–dimension relationships: results from mc3e," Atmos. Chem. Phys. **19**, 3621–3643 (2019).
[17]D. J. Posselt, F. He, J. Bukowski, and J. S. Reid, "On the relative sensitivity of a tropical deep convective storm to changes in environment and cloud microphysical parameters," J. Atmos. Sci. **76**, 1163–1185 (2019).
[18]A. Cauteruccio, M. Colli, M. Stagnaro, L. G. Lanza, and E. Vuerich, "In-situ precipitation measurements," (Springer International Publishing, 2021) pp. 359–400.
[19]J. Grazioli, G. Ghiggi, A.-C. Billault-Roux, and A. Berne, "Mascdb, a database of images, descriptors and microphysical properties of individual snowflakes in free fall," Scientific data **9**, 1–16 (2022).
[20]E. Bou-Zeid, W. Anderson, G. G. Katul, and L. Mahrt, "The persistent challenge of surface heterogeneity in boundary-layer meteorology: a review," Boundary-Layer Meteorology **177**, 227–245 (2020).
[21]T. Zeugin, Q. Krol, I. Fouxon, and M. Holzner, "Sedimentation of snow particles in still air in stokes regime," Geophy. Res. Lett. **47**, e2020GL087832 (2020).
[22]P. K. Wang, *Motions of ice hydrometeors in the atmosphere: Numerical studies and implications* (Spinger, 2021).
[23]M. W. McCorquodale and C. D. Westbrook, "Trail part 2: A comprehensive assessment of ice particle fall speed parametrisations," Q. J. R. Meteorol. Soc. **147**, 605–626 (2021).
[24]S. Elghobashi, "On predicting particle-laden turbulent flows," Appl. Sci. Res. **52**, 309–329 (1994).
[25]V. Mathai, V. N. Prakash, J. Brons, C. Sun, and D. Lohse, "Wake-driven dynamics of finite-sized buoyant spheres in turbulence," Phy. Rev. lett. **115**, 124501 (2015).
[26]A. Nemes, T. Dasari, J. Hong, M. Guala, and F. Coletti, "Snowflakes in the atmospheric surface layer: observation of particle–turbulence dynamics," J. Fluid. Mech. **814**, 592–613 (2017).
[27]J. Li, A. Abraham, M. Guala, and J. Hong, "Evidence of preferential sweeping during snow settling in atmospheric turbulence," J. Fluid. Mech. **928** (2021).
[28]M. Maxey, "The motion of small spherical particles in a cellular flow field," Phys. Fluid. **30**, 1915–1928 (1987).
[29]J. Li, M. Guala, and J. Hong, "Snow particle analyzer for simultaneous measurements of snow density and morphology," arXiv preprint arXiv:2209.11129 (2022).
[30]D. K. Singh, E. R. Pardyjak, and T. J. Garrett, "Time-resolved measurements of the densities of individual frozen hydrometeors and of fresh snowfall," Atmos. Meas. Tech. (2023), DOI: 10.5194/amt-2023-148.
[31]D. K. Singh, S. Donovan, E. R. Pardyjak, and T. J. Garrett, "A differential emissivity imaging technique for measuring hydrometeor mass and type," Atmos. Meas. Tech. **14**, 6973–6990 (2021).
[32]T. I. Alcott and W. J. Steenburgh, "Snow-to-liquid ratio variability and prediction at a high-elevation site in utah's wasatch mountains," Weather. Forecast. **25**, 323–337 (2010).
[33]J. Hong, M. Toloui, L. P. Chamorro, M. Guala, K. Howard, S. Riley, J. Tucker, and F. Sotiropoulos, "Natural snowfall reveals large-scale flow structures in the wake of a 2.5-mw wind turbine," Nat. Commun. **5**, 1–9 (2014).
[34]R. Hassanian, A. Helgadottir, L. Bouhlali, and M. Riedel, "An experiment generates a specified mean strained rate turbulent flow: Dynamics of particles," Physics of Fluids **35** (2023).
[35]F. D. Dimotakis, P. E. Debussy and M. M. Koochesfahani, "Particle streak velocity field measurements in a two-dimensional mixing layer," Phys. Fluid. **24**, 995 (1981).
[36]H. P. Böhm, "A general equation for the terminal fall speed of solid hydrometeors," J. Atmos. Sci. **46**, 2419–2427 (1989).
[37]A. J. Heymsfield and C. Westbrook, "Advances in the estimation of ice particle fall speeds using laboratory and field measurements," J. Atmos. Sci. **67**, 2469–2482 (2010).
[38]T. J. Morrison, T. Meisenheimer, T. Garrett, D. Singh, S. Donovan, and E. Pardyjak, "Relating storm-snow avalanche instabilities to data collected from the differential emissivity imaging disdrometer (deid)," Cold Regions Science and Technology **210**, 103839 (2023).
[39]C. Fierz, R. L. Armstrong, Y. Durand, P. Etchevers, E. Greene, D. M. McClung, K. Nishimura, P. K. Satyawali, and S. A. Sokratov, "The international classification for seasonal snow on the ground," (2009).
[40]G. A. Voth, A. La Porta, A. M. Crawford, J. Alexander, and E. Bodenschatz, "Measurement of particle accelerations in fully developed turbulence," J. Fluid. Mech. **469**, 121–160 (2002).
[41]J. Bec, L. Biferale, G. Boffetta, A. Celani, M. Cencini, A. Lanotte, S. Musacchio, and F. Toschi, "Acceleration statistics of heavy particles in turbulence," J. Fluid. Mech. **550**, 349–358 (2006).
[42]M. Bini and W. P. Jones, "Particle acceleration in turbulent flows: A class of nonlinear stochastic models for intermittency," Physics of Fluids **19**, 035104 (2007).
[43]Y. Lin and H. Xu, "Experimental investigation of pressure statistics in laboratory homogeneous isotropic turbulence," Physics of Fluids **35** (2023).
[44]A. La Porta, G. A. Voth, A. M. Crawford, J. Alexander, and E. Bodenschatz, "Fluid particle accelerations in fully developed turbulence," Nature **409**, 1017–1019 (2001).
[45]J. M. Mercado, V. N. Prakash, Y. Tagawa, C. Sun, and D. Lohse, "Lagrangian statistics of light particles in turbulence," Phys. Fluid. **24**, 055106 (2012).
[46]S. Vajedi, K. Gustavsson, B. Mehlig, and L. Biferale, "Inertial-particle accelerations in turbulence: a lagrangian closure," J. Fluid. Mech. **798**, 187–200 (2016).
[47]N. M. Qureshi, U. Arrieta, C. Baudet, A. Cartellier, Y. Gagne, and M. Bourgoin, "Acceleration statistics of inertial particles in turbulent flow," Europ. Phys. J. B **66**, 531–536 (2008).
[48]G. A. Voth, K. Satyanarayan, and E. Bodenschatz, "Lagrangian acceleration measurements at large reynolds numbers," Phys. Fluid. **10**, 2268–2280 (1998).
[49]G. Gulitski, M. Kholmyansky, W. Kinzelbach, B. Lüthi, A. Tsinober, and S. Yorish, "Velocity and temperature derivatives in high-reynolds-number turbulent flows in the atmospheric surface layer. part 3. temperature and joint statistics of temperature and velocity derivatives," Journal of Fluid Mechanics **589**, 103–123 (2007).

[50]A. N. Kolmogorov, "The local structure of turbulence in incompressible viscous fluid for very large Reynolds numbers," Dokl. Akad. Nauk. SSSR. (1941), reprinted in Proc. R. Soc. London, Ser. A **434**(9), (1991).
[51]W. Heisenberg, "Zur statistischen theorie der turbulenz," Zeitschrift für Physik **124**, 628–657 (1948).
[52]R. A. Shaw and S. P. Oncley, "Acceleration intermittency and enhanced collision kernels in turbulent clouds," Atmos. Res. **59**, 77–87 (2001).
[53]G. Gulitski, M. Kholmyansky, W. Kinzelbach, B. Lüthi, A. Tsinober, and S. Yorish, "Velocity and temperature derivatives in high-reynolds-number turbulent flows in the atmospheric surface layer. part 1. facilities, methods and some general results," J. Fluid. Mech. **589**, 57–81 (2007).
[54]P. J. Ireland, A. D. Bragg, and L. R. Collins, "The effect of reynolds number on inertial particle dynamics in isotropic turbulence. part 2. simulations with gravitational effects," J. Fluid. Mech. **796**, 659–711 (2016).
[55]V. Mathai, E. Calzavarini, J. Brons, C. Sun, and D. Lohse, "Microbubbles and microparticles are not faithful tracers of turbulent acceleration," Phy. Rev. lett. **117**, 024501 (2016).
[56]D. Buaria and K. R. Sreenivasan, "Scaling of acceleration statistics in high reynolds number turbulence," Phy. Rev. lett. **128**, 234502 (2022).
[57]U. Nakaya, "Snow crystals," in *Snow Crystals* (Harvard University Press, 2013).
[58]T. J. Garrett, "Analytical solutions for precipitation size distributions at steady state," J. Atmos. Sci. **76**, 1031–1037 (2019).
[59]K. N. Rees, D. K. Singh, E. R. Pardyjak, and T. J. Garrett, "Mass and density of individual frozen hydrometeors," Atmos. Chem. Phys. **21**, 14235–14250 (2021).
[60]A. A. Grachev, L. S. Leo, S. D. Sabatino, H. J. Fernando, E. R. Pardyjak, and C. W. Fairall, "Structure of turbulence in katabatic flows below and above the wind-speed maximum," Boundary-layer meteorology **159**, 469–494 (2016).
[61]C. Hang, D. F. Nadeau, E. R. Pardyjak, and M. B. Parlange, "A comparison of near-surface potential temperature variance budgets for unstable atmospheric flows with contrasting vegetation cover flat surfaces and a gentle slope," Environmental Fluid Mechanics **20**, 1251–1279 (2020).
[62]L. Benedict and R. Gould, "Towards better uncertainty estimates for turbulence statistics," Experiments in fluids **22**, 129–136 (1996).